JOURNAL OF AIRCRAFT
Vol. 40, No. 4, July–August 2003

Wind Estimation on a Lightweight Vertical-Takeoff- and-Landing Uninhabited Vehicle

Nicola de Divitiis*
University of Rome "La Sapienza," 00184 Rome, Italy

Wind-velocity measurement on a rotary-wing aircraft is a difficult task because of the flow induced by the rotors. The purpose of this paper is to develop a method to estimate the wind velocity components from the measurement of the state variables of a rotorcraft in the moving atmosphere. The algorithm presented is in the framework of the output error method. The wind-velocity components were estimated using a novel variational formulation. The method uses airframe and rotor models that calculate the aerodynamic and thrust coefficients by means of an artificial neural-network technique. To validate the method, the results are compared to wind-velocity estimates from a Kalman–Bucy filter.

Nomenclature

$\boldsymbol{A}$	=	state matrix
$\boldsymbol{a} \equiv (a_{Wx}, a_{Wy}, a_{Wz})$	=	wind acceleration in the inertial frame
a_x, a_y, a_z	=	vehicle acceleration components in body axes
$\boldsymbol{B}$	=	control matrix
$\boldsymbol{C} \equiv \partial \boldsymbol{h}/\partial \boldsymbol{x}$	=	observability state matrix
C_l, C_m, C_n	=	aerodynamic moment coefficients
$C_{l_T}, C_{m_T}, C_{n_T}$	=	rotor moment coefficients
C_x, C_y, C_z	=	aerodynamic force coefficients
$C_{x_T}, C_{y_T}, C_{z_T}$	=	thrust force coefficients
D	=	fuselage diameter
$\boldsymbol{D} \equiv \partial \boldsymbol{h}/\partial \boldsymbol{u}$	=	observability control matrix
$\boldsymbol{F} \equiv \partial \boldsymbol{f}/\partial \boldsymbol{\eta}$	=	state noise matrix
$\boldsymbol{f}$	=	right-hand side of the equations of motion
$f(x)$	=	neural-network activation function
$\boldsymbol{f}^s$	=	stabilized right-hand side of the equations of motion
g	=	gravity acceleration
$\boldsymbol{g}$	=	observability function
$\boldsymbol{H} \equiv \partial \boldsymbol{f}/\partial \boldsymbol{w}$	=	state wind matrix
$\boldsymbol{h}$	=	Kalman-filter observability function
I_x, I_y, I_z	=	principal moments of inertia
I_{xz}	=	product of inertia
J	=	merit function
$\boldsymbol{K}$	=	steady-state Kalman matrix gain
$k = V/\lvert v_R - V \sin\alpha \rvert$	=	velocity parameter
L, M, N	=	aerodynamic moment components
L_T, M_T, N_T	=	rotor moment components
$\boldsymbol{P} \equiv \langle x_i x_j \rangle$	=	covariance state matrix
p, q, r	=	angular velocity components in body axes
R	=	rotor radius
$\boldsymbol{R} \equiv \langle \xi_i \xi_j \rangle$	=	covariance measurement matrix
S	=	rotorcraft reference surface
$\boldsymbol{u} \equiv (\delta_A, \delta_B, \delta_C, \delta_P)$	=	control vector
V	=	velocity modulus
$\boldsymbol{V} = \langle \eta_i \eta_j \rangle$	=	covariance dynamic matrix
$\boldsymbol{v} \equiv (u, v, w)$	=	inertial velocity in body axes
v_R	=	rotor-induced velocity
W	=	weight
$\boldsymbol{w} \equiv (u_g, v_g, w_g)$	=	wind velocity in the inertial frame
X, Y, Z	=	aerodynamic force components
X_T, Y_T, Z_T	=	thrust force components
x, y, z	=	inertial coordinates
$\boldsymbol{x}$	=	state vector
$\boldsymbol{y}$	=	observation vector
$\boldsymbol{z}$	=	measurement vector
α	=	angle of attack
$\boldsymbol{\Gamma}$	=	optimum matrix gain
$\gamma = V/\Omega R$	=	advance ratio
δ_A	=	lateral cyclic control, positive right
δ_B	=	longitudinal cyclic control, positive after
δ_C	=	collective control, positive up
δ_P	=	differential collective control, positive right
$\boldsymbol{\eta}$	=	state noise vector
$\boldsymbol{\xi}$	=	measurement noise vector
ρ	=	air density
$\sigma_x, \sigma_y, \sigma_z$	=	wind-velocity standard deviations
φ, ϑ, ψ	=	Euler angles
Ω	=	rotor angular velocity
$\langle \cdot \rangle$	=	mean value

Subscripts

a	=	augmented value
e	=	estimated value
NN	=	neural network

Superscript

T	=	transpose

Introduction

In the last decade the development of the unmanned aerial vehicle (UAV) was a result of the increasing use of this kind of vehicle in different fields of application.[1] These UAV applications require estimation of the local atmospheric wind through measurements realized on vehicle.

The difficulties to measure the local wind velocities in various regions at different altitudes yield the wind estimation by measurements on board on the aircraft a subject of increasing interest.

In particular, it is difficult to carry out wind measurements on a rotary-wing vehicle because of the strong perturbation caused from the flow induced by the rotors on the aerodynamic field about the airframe. This is the main motivation of the present study, the

Received 16 August 2002; revision received 21 April 2003; accepted for publication 21 April 2003.

*Research Fellow, Department of Mechanics and Aeronautics, via Eudossiana, 18.

Table 1 Characteristics of the UAV

Characterstic	Value
Overall diameter, m	1.9
Rotor diameter, m	1.1
Central hub diameter, m	0.25
Maximum overall weight, N	800
Payload, N	100
Coaxial rotors	2
Power, h.p.	3×14
at, RPM	11,000
Rotor speed, RPM	3,000
Endurance, h	1.5
Service ceiling, m	2,000

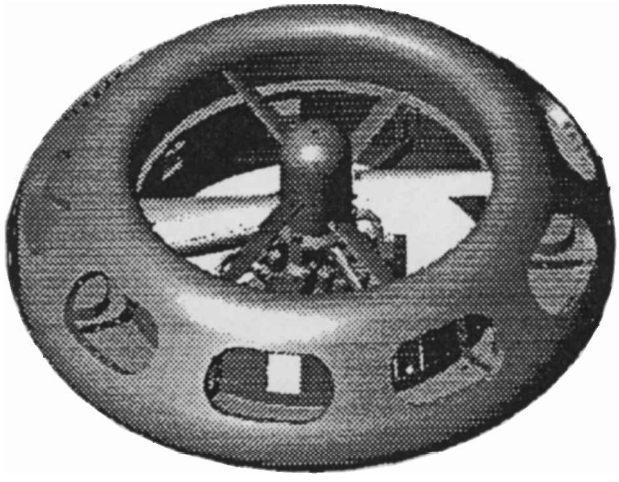

Fig. 1 Three-dimensional view of the UAV.

purpose of which is to develop a procedure for the estimation of the wind-velocity components through the measurements of the state variables of a vertical-takeoff-and-landing uninhabited aerial vehicle (UAV).

The UAV addressed in the present study is a shrouded-fan rotorcraft shown in Fig. 1, the principal characteristics of which are reported in Table 1. The vehicle is the result of a research project jointly developed from the University of Rome "La Sapienza" and the Polytechnic of Turin.[2,3]

The aerial platform is powered by two counter-rotating three-blade rotors, placed at the center of the toroidal fuselage, driven by three two-stroke air-cooled engines. The configuration is rather peculiar from the aerodynamic point of view because of the strong interaction between the rotor-induced flow and the body aerodynamics.

The aerodynamic force and moment developed by the rotorcraft airframe are calculated by means of the method proposed in Ref. 2, which requires the definition of a Lagrangian function representing the kinetic energy of the flow expressed in terms of the UAV state variables and allows the calculation of aerodynamic forces and moments through the method of the Lagrange equations.[4]

As for the propulsive actions, the same model used in Refs. 2 and 3 is adopted here.

Although there are a number of references in the literature regarding wind estimation, to the author's knowledge the determination of wind through the observation of vehicle state variables has not received great attention. A work on wind velocities identification is from Katz and Sharma.[5] They consider an aircraft flying in coordinated flight into a constant and horizontal wind and proposes an algorithm for wind-velocity calculation that relies on the observation of vehicle state variables. Katz demonstrates a theorem that guarantees the convergence of his method in the sense that the estimated wind velocity monotonically approaches the true wind velocity. The algorithm, which has flight speed and Euler angles as observed variables, is based on a filtering technique and can be applied in a steady maneuver.

In a more realistic situation where instantaneous maneuvers are performed in a variable wind, the estimation cannot be limited to coordinated flight conditions, but it must take into account the effects of vehicle dynamics and wind unsteadiness.

The basic idea of the present study is that the wind-velocity components can be considered as characteristic parameters of the vehicle because they appear in the force and moment equations. Hence, different identification methods can be applied[6,7] to estimate the wind velocity from state variables measurement. From a theoretical standpoint the wind velocity can be estimated through the instantaneous observation of state variables and linear acceleration components.[8,9]

In this framework McCool et al., in a work dealing with the estimation of sideslip angle of a helicopter flying at very low airspeed, evaluates the feasibility of neural-network techniques to determine the sideslip angle and, in order to find the neural-network architecture which provides better results, analyzes several neural-network configurations.

The algorithms based on the neural-network technique are also applied to determine the state variables in the flight-test programs, where, because of the wear and degradation of the instrumentation, the measurements realized during the flights are influenced by errors. In this context McMillen et al.[9] apply the neural network technique to flight-test data to determine several quantities such as the aerodynamic angles, the Euler angles, and the control deflections and shows that it is often necessary to employ a single network for each unknown parameter to achieve a correct identification.

In this study an algorithm, based on a variational technique (VT), is proposed for the wind estimation on the aforementioned UAV model. The procedure, which requires the definition of a merit function J as a quadratic form of the difference between measured and estimated observable variables, is in the framework of the output error method, which can be regarded, in short, as a nonlinear minimization procedure that is commonly used for the identification of vehicle parameters.[6,7]

The measured state variables are generated from direct simulations of the UAV motion, whereas the estimated observable variables are determined by means of a vehicle mathematical model that incorporates artificial neural networks for the estimation of aerodynamic and thrust coefficients.

The main feature of the VT consists in the introduction of adjoint differential equations, which reasonably describe the time evolution of wind velocities. The right-hand side (RHS) of this differential system presents several unknown parameters that are related to the time variations of the wind-velocity components. These new equations are the constraints of the optimal problem, and the unknown parameters are determined through the minimization of J.

To assess the performance of the novel method, the results obtained by the VT approach are compared with those of a classic technique based on the filtering approach, where the wind-velocity components are determined as an augmented state using a steady-state extended Kalman–Bucy filter (KF).[6,7]

Rotorcraft

To generate simulated flight-test data, a full nonlinear six-degree-of-freedom model of the vehicle is now defined. The equations of motion of the rigid vehicle are written as follows[10]:

$$\dot{u} = g\frac{X_T + X}{W} - g\sin\vartheta - qw + rv, \qquad \dot{v} = g\frac{Y_T + Y}{W} + g\cos\vartheta\sin\varphi - ru + pw, \qquad \dot{w} = g\frac{Z_T + Z}{W} + g\cos\vartheta\cos\varphi - pv + qu,$$

$$\dot{\varphi} = p + \sin\varphi\tan\vartheta q + \cos\varphi\tan\vartheta r, \qquad \dot{\vartheta} = \cos\varphi q - \sin\varphi r, \qquad \dot{\psi} = \sin\varphi\sec\vartheta q + \cos\varphi\sec\vartheta r$$

$$p = \frac{[I_{xz}pq + (I_y - I_z)qr + L + L_T]I_z + [-I_{xz}qr + (I_x - I_y)pq + N + N_T]I_{xz}}{I_x I_z - I_{xz}^2}, \qquad q = \frac{I_{xz}(r^2 - p^2) + (I_z - I_x)pr + M + M_T}{I_y}$$

$$r = \frac{[-I_{xz}qr + (I_x - I_y)pq + N + N_T]I_x + [I_{xz}pq + (I_y - I_z)qr + L + L_T]I_{xz}}{I_x I_z - I_{xz}^2}$$

$$\begin{aligned} \dot{x} &= (\cos\vartheta\cos\psi)u + (\sin\varphi\sin\vartheta\cos\psi - \cos\varphi\sin\psi)v + (\cos\varphi\sin\vartheta\cos\psi + \sin\varphi\sin\psi)w \\ \dot{y} &= (\cos\vartheta\sin\psi)u + (\sin\varphi\sin\vartheta\sin\psi + \cos\varphi\cos\psi)v + (\cos\varphi\sin\vartheta\sin\psi - \sin\varphi\cos\psi)w \\ \dot{z} &= (-\sin\vartheta)u + (\sin\varphi\cos\vartheta)v + (\cos\varphi\cos\vartheta)w \end{aligned} \tag{1}$$

where the aerodynamic and thrust force and moment terms in Eqs. (1) are expressed in the following two sections.

Vehicle Aerodynamics

Because of the complexity of the flow around the rotorcraft, together with the strong interaction between fan flow and aerodynamic field about the fuselage, the determination of the fuselage aerodynamic coefficients is a difficult task.

To determine the aerodynamic force and moment developed by the UAV fuselage, the aerodynamic model proposed in Ref. 2 is here adopted. This model, based on a potential representation of the flowfield around the vehicle, consists of a Lagrangian approach whose peculiarity is to derive the aerodynamic force and moment through the Lagrange equations method[4] applied to a Lagrangian function T, which represents the kinetic energy of the stream. The model yields the mathematical expressions of the aerodynamic coefficients in terms of the angle of attack α, of the velocity parameter $k = V/|v_R - V\sin\alpha|$, and of the three angular velocities.

Therefore, the aerodynamic force and moment on the fuselage are obtained using the Lagrange equations in the general form[2,4]

$$(X, Y, Z) = -\frac{\mathrm{d}}{\mathrm{d}t}\frac{\partial T}{\partial \boldsymbol{v}} - \boldsymbol{\omega} \times \frac{\partial T}{\partial \boldsymbol{v}}$$

$$(L, M, N) = -\boldsymbol{v} \times \frac{\partial T}{\partial \boldsymbol{v}} - \frac{\mathrm{d}}{\mathrm{d}t}\frac{\partial T}{\partial \boldsymbol{\omega}} - \boldsymbol{\omega} \times \frac{\partial T}{\partial \boldsymbol{\omega}} \tag{2}$$

where as the corresponding aerodynamic coefficients are defined by

$$(X, Y, Z) = \tfrac{1}{2}\rho V_f^2 S(C_x, C_y, C_z)$$

$$(L, M, N) = \tfrac{1}{2}\rho V_f^2 SD(C_l, C_m, C_n) \tag{3}$$

where D is the shroud diameter, $S = \pi D^2/4$ is the reference surface and

$$V_f = \sqrt{(u - u_g)^2 + (v - v_g)^2 + (w - w_g - v_R)^2} \tag{4}$$

is the reference velocity.

The expression of T contains several unknown parameters[2] that give the aerodynamic characteristics of the vehicle. These quantities, which are the free parameters of the model, have been identified through the elaboration of the data calculated by the code VSAERO,[11] which is capable of solving the complex aerodynamic field on the airframe in the presence of the fan flow.

As a result of the vehicle symmetry about the z axis, the flow on the shroud depends upon α and k, and, therefore, Eqs. (2) and (3) yield aerodynamic coefficients that are functions of α, k and p, q, r and do not depend on sideslip angle.

The model is able to take into account the aforementioned effects of interaction between the rotor flow and the aerodynamic field about the vehicle.

Rotor

The aerodynamic actions developed by the rigid (no flapping) counter-rotating rotors provide lift force and control moments to manage rotorcraft attitude. In particular, pitch and roll are controlled through longitudinal δ_B and lateral δ_A variations of blade pitch, whereas the yaw control is carried out by means of differential variation δ_P of the collective pitch on both rotors whose angular velocity is kept constant by a rpm governor. The blade pitch is controlled by a mechanism consisting of two independent swash plates, each driven by three actuators. Rigid rotors cause moments that are transmitted to the fuselage and, because they have the same moments of inertia with respect to their rotation axis, the gyroscopic effects of the two rotors are balanced by each other and therefore do not appear in the rigid-body moment equations.

The thrust forces and moments developed by the rotors are given by the equations[12]

$$(X_T, Y_T, Z_T) = -\pi\rho\Omega^2 R^4 (C_{x_T}, C_{y_T}, C_{z_T})$$

$$(L_T, M_T, N_T) = \pi\rho\Omega^2 R^5 (C_{l_T}, C_{m_T}, C_{n_T}) \tag{5}$$

The rotor model, based on the blade-element theory, calculates the thrust and moment coefficients through analytical integration of the aerodynamic load along the blade span assuming steady-state aerodynamics, whereas the effects from the blade-tip losses and the mutual influence between the two rotors are neglected. As a consequence, the rotor coefficients depend on angle of attack α, advance ratio γ, angular velocity (p, q, r), and the control deflections $(\delta_A, \delta_B, \delta_C, \delta_P)$.

Neural-Network-Based Vehicle Model

To estimate the wind-velocity components by the measurements of the observable variables, it is necessary to have a vehicle mathematical model that estimates the time derivatives of the state variables in terms of the state and control variables and wind velocity. This model is realized by means of the neural-network technique.

Very often the neural networks are utilized to model the entire vehicle model equations, which, in turn, includes well-known terms such as the weight components and the moments of the inertia forces.

Here the equations of motion, forces, and moments acting on the rotorcraft are given by Eqs. (1), (3), and (5), respectively, where each aerodynamic or thrust coefficient is expressed by means of artificial neural-networks' technique.

According to Ref. 9, each neural network is used to determine a single aerodynamic or rotor thrust and moment coefficient. The input variables are the pairs (α, k) for the aerodynamic coefficients and (α, γ) for the rotor actions.

The contribution of the controls and the angular velocity is taken into account, respectively, through the control derivatives and the derivatives with respect to p, q, and r.

Figure 2 illustrates the neural-network architecture here utilized that consists in a feed-forward scheme where each layer is completely connected to its contiguous one. The input layer has two neurons, each employing a linear activation function, and it is fully connected with the first hidden layer. The neurons of each hidden layer have the hyperbolic tangent as activation function

$$f(x) = \frac{e^x - e^{-x}}{e^x + e^{-x}} \tag{6}$$

and simple multiplicative connection with weight w_{ij} is realized between two generic neurons ith and jth so that the signal at the ith neuron results[9]:

$$x_i = f\left(\sum_j w_{ij} x_j\right) \tag{7}$$

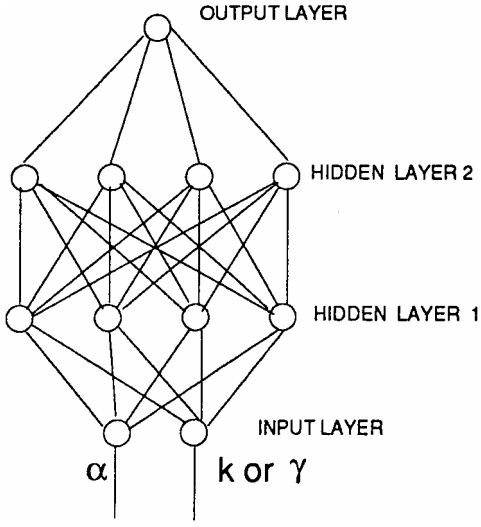

Fig. 2 Schematic of the artificial neural-network architecture.

All of the networks have two hidden layers, whereas the output layer is made of a single neuron, which corresponds to a simple linear activation function. The number of neurons for each hidden layer is selected in such a way that the maximum difference between estimated and real value is less than 1% of the maximum value. In this respect tests show that the number of neurons for each hidden layer which satisfy this condition is greater than 18. Hence all of the networks have two hidden layers with 20 neurons.

To train the neural networks, the aerodynamic and rotor models described in the preceding sections have been used to generate 40,000 randomly generated pairs (α, k) or (α, γ) with an uniform probability distribution in the intervals $(-90, 90) \times (0, 2)$ or $(-90, 90) \times (-0.5, 0.5)$, respectively. Each single neural network is trained by presenting to it all of the aforementioned pairs and the corresponding coefficients.

The artificial neural networks are used only to estimate the aerodynamic and rotor coefficients in a preprocessing step followed by wind estimation.

Aerodynamic Model

Each aerodynamic coefficient C_i is supposed to be the sum of a part $C_{i\,\mathrm{NN}}$ that depends on α and k, plus linear functions of p, q, and r, that is,

$$C_i = C_{i\,\mathrm{NN}}(\alpha, k) + \frac{\partial C_i}{\partial p}p + \frac{\partial C_i}{\partial q}q + \frac{\partial C_i}{\partial r}r \qquad (i = x, y, z, l, m, n) \quad (8)$$

where $(p, q, r) = D/2V(p, q, r)$. The first term of Eq. (8) is modeled using an artificial neural network (Fig. 2) that has α and k as input parameters and the aerodynamic coefficients evaluated at $p = q = r = 0$ as outputs. The other terms represent the contributions of the rotary derivatives to the aerodynamic coefficients. Each rotary derivative is a function of α and k and is expressed through the terms of Eq. (2) that depend on p, q, and r.

Rotor Model

Rotor thrust and moment coefficients depend upon $\alpha, \gamma, (p, q, r)$ and $(\delta_A, \delta_B, \delta_C, \delta_P)$, and, also in this case, they are expressed as

$$C_{iT} = C_{i\mathrm{TNN}}(\alpha, \gamma) + \frac{\partial C_{iT}}{\partial p}p + \frac{\partial C_{iT}}{\partial q}q + \frac{\partial C_{iT}}{\partial r}r + \frac{\partial C_{iT}}{\partial \delta_A}\delta_A + \frac{\partial C_{iT}}{\partial \delta_B}\delta_B + \frac{\partial C_{iT}}{\partial \delta_C}\delta_C + \frac{\partial C_{iT}}{\partial \delta_P}\delta_P \qquad (i = x, y, z, l, m, n) \quad (9)$$

where the rotary and control derivatives are assumed to be constant quantities, whereas the expressions of the nonlinear functions $C_{i\,\mathrm{TNN}}$ are obtained through a neural network, which has the same scheme shown in Fig. 2.

State Representation and Observability

Both rotorcraft and the vehicle neural-network model are in the state-space form. The equations of motion for the rotorcraft can be written as

$$\boldsymbol{x} = \boldsymbol{f}(\boldsymbol{x}, \boldsymbol{u}, \boldsymbol{w}, \boldsymbol{\eta})$$

$$\boldsymbol{y} = \boldsymbol{g}(\boldsymbol{x}, \boldsymbol{x}, \boldsymbol{u}) \equiv \boldsymbol{g}[\boldsymbol{x}, \boldsymbol{f}(\boldsymbol{x}, \boldsymbol{u}, \boldsymbol{w}, \boldsymbol{\eta}), \boldsymbol{u}], \qquad \boldsymbol{z} = \boldsymbol{y} + \boldsymbol{\xi} \quad (10)$$

where $\boldsymbol{x} = (u, v, w, \varphi, \vartheta, \psi, p, q, r, x, y, z)$ is the state vector, the function $\boldsymbol{f}$ represents the RHS of the motion equations wherein aerodynamic and thrust coefficients are calculated as described in the proper sections, whereas $\boldsymbol{y}$ and $\boldsymbol{z}$ define, respectively, the observability and measurability of the dynamical system. The measurement noise $\boldsymbol{\xi}$ is caused by the instrumentation errors, whereas $\boldsymbol{\eta}$ can have various origins such as the engine vibrations or the air turbulence. In the latter case $\boldsymbol{w}$ and $\boldsymbol{\eta}$ are, respectively, the average wind-velocity and the wind-velocity fluctuations.

The present analysis prescribes the observability of $\boldsymbol{x}$ and $\boldsymbol{x}$ so that $\boldsymbol{y}$ depends on $\boldsymbol{x}$, $\boldsymbol{u}$, $\boldsymbol{w}$ and $\boldsymbol{\eta}$.

As for the neural-network model,

$$\boldsymbol{x}_e = \boldsymbol{f}_{\mathrm{NN}}(\boldsymbol{x}, \boldsymbol{u}, \boldsymbol{w}_e) \quad (11)$$

$$\boldsymbol{y}_e = \boldsymbol{g}(\boldsymbol{x}, \boldsymbol{x}_e, \boldsymbol{u}) \equiv \boldsymbol{g}_{\mathrm{NN}}(\boldsymbol{x}, \boldsymbol{u}, \boldsymbol{w}_e) \quad (12)$$

where $\boldsymbol{f}_{\mathrm{NN}}$ is the RHS of the equations of motion wherein the aerodynamic and thrust coefficients are given by neural networks while $\boldsymbol{y}_e$ and $\boldsymbol{w}_e$ are the estimated output quantities and the estimated wind velocity.

Although Eq. (11) is not used to calculate the time history of the state variables, it is necessary to determine $\boldsymbol{x}_e$ as the function of $\boldsymbol{x}$, $\boldsymbol{u}$, and $\boldsymbol{w}_e$ to obtain the estimated observable variables in terms of $\boldsymbol{x}$, $\boldsymbol{u}$, and $\boldsymbol{w}_e$.

Stability Augmentation

The vehicle is highly unstable, and its dynamic characteristics are significantly influenced by the flight velocity and the angle of attack.[3] Therefore, a control system is to be designed for its stabilization in a wide range of flight conditions. The linear quadratic regulator technique is here adopted for the sake of simplicity, where the matrix gain $\boldsymbol{\Gamma}$ is determined, which gives a minimum value for the performance integral[13]

$$\int_0^\infty \left(\boldsymbol{\Delta x}^T \boldsymbol{Q}_w \boldsymbol{\Delta x} + \boldsymbol{\Delta u}^T \boldsymbol{R}_w \boldsymbol{\Delta u}\right) \mathrm{d}t \quad (13)$$

where $\boldsymbol{\Delta u} = -\boldsymbol{\Gamma \Delta x}$, $\boldsymbol{Q}_w$, and $\boldsymbol{R}_w$ are the state weighting and control weighting matrices respectively, and $\boldsymbol{\Delta}$ indicates perturbations with respect to the reference condition. The control command is expressed as

$$\boldsymbol{u} = \boldsymbol{u} - \boldsymbol{\Gamma \Delta x} \quad (14)$$

where $\boldsymbol{\Gamma}$ is given by

$$\boldsymbol{\Gamma} = \boldsymbol{R}_w^{-1} \boldsymbol{B}^T \boldsymbol{M} \quad (15)$$

being $\boldsymbol{M}$ the solution of the steady-state Riccati equation

$$\boldsymbol{MA} + \boldsymbol{A}^T \boldsymbol{M} - \boldsymbol{MBR}_w^{-1} \boldsymbol{B}^T \boldsymbol{M} + \boldsymbol{Q}_w = 0 \quad (16)$$

where $\boldsymbol{A}$ and $\boldsymbol{B}$, which are obtained from Eqs. (11), are numerically calculated by centered finite differences, and Eq. (16) is solved using a Newton–Raphson algorithm.

Therefore, the control law is implemented on the rotorcraft as follows:

$$\boldsymbol{x} = \boldsymbol{f}(\boldsymbol{x}, \boldsymbol{u} - \boldsymbol{\Gamma \Delta x}, \boldsymbol{w}, \boldsymbol{\eta}) \equiv \boldsymbol{f}^s(\boldsymbol{x}, \boldsymbol{u}, \boldsymbol{w}, \boldsymbol{\eta}) \quad (17)$$

The calculation of Γ is only valid around the reference conditions. Some tests have shown that the typical scheduling of $\boldsymbol{Q}_w$ and $\boldsymbol{R}_w$ with slow state variables such as airspeed and altitude cannot be sufficient to stabilize the rotorcraft in the various flight situations because of the strong nonlinearity of the model. For this reason, during the simulation the matrices $\boldsymbol{A}$, $\boldsymbol{B}$, and Γ are updated when the maximum of the state variables variations exceeds the 10% of their reference values. These reference values, which are selected in order to stabilize the vehicle, are V_f for the velocity components, $0.01(V_f/D)$ for the angular velocity components, and $\pi/2$ for the Euler angles.

In the calculations $\boldsymbol{Q}_w$ and $\boldsymbol{R}_w$ are given by the values $Q_{w11} = Q_{wij} = 0$, $(i \neq j)$, $Q_{w22} = Q_{w33} = 1/V_{\mathrm{REF}}$, $Q_{w44} = Q_{w55} = Q_{w66} = Q_{w77} = Q_{w88} = Q_{w99} = 1$, and $R_{wij} = 0$, $(i \neq j)$, $R_{wii} = 1$, $(i = 1, 2, 3, 4)$.

Variational Technique for Wind-Velocity Estimation

The procedure illustrated in this section is founded on a variational technique, the characteristics of which are in the framework of output error method that, basically, consists of nonlinear optimization procedures and is commonly employed to estimate the parameters of aircraft model.[6,7]

In this study the minimum of the following functional is searched for:

$$J(\boldsymbol{w}) = \frac{1}{2T}\int_0^T [\boldsymbol{z}(t) - \boldsymbol{y}_e]^T \boldsymbol{R}^{-1}[\boldsymbol{z}(t) - \boldsymbol{y}_e]\,\mathrm{d}t \tag{18}$$

which depends, through Eq. (12), upon $\boldsymbol{w}_e$.

The solution that minimizes J supplies an estimation of the wind velocity $\boldsymbol{w}_e$ that, as shows from Eq. (18), directly depends on the covariance matrix $\boldsymbol{R}$.

The condition that leads to the minimum of J can be expressed using variational calculus $\delta L = (\partial J^T/\partial \boldsymbol{w}_e)\delta \boldsymbol{w}_e = 0 \;\forall\, \delta \boldsymbol{w}_e$. Because of the arbitrariness of $\delta \boldsymbol{w}_e$, one obtains

$$\frac{\partial J}{\partial \boldsymbol{w}_e} \equiv \frac{1}{T}\int_0^T \boldsymbol{R}^{-1}\frac{\partial \boldsymbol{g}_{\mathrm{NN}}}{\partial \boldsymbol{w}_e}\,\mathrm{d}t = 0 \tag{19}$$

The solution of Eq. (19) only exists if $\boldsymbol{R}$ is not singular and, $\partial \boldsymbol{g}_{\mathrm{NN}}/\partial \boldsymbol{w}_e \neq 0$ and provides the time variations $\boldsymbol{w}_e$ during the observation period T.

Several numerical methods can be used to solve Eq. (19). Actually the minimization is carried out by introducing, together with Eq. (18), a set of differential equations that reasonably represents the time history of the wind velocities

$$\boldsymbol{w}_e = \boldsymbol{a} \equiv (a_{Wx}, a_{Wy}, a_{Wz}), \qquad \sqrt{\boldsymbol{a}^T\boldsymbol{a}} \leq a_{\mathrm{MAX}} \tag{20}$$

where the RHS $\boldsymbol{a}$ is the a priori unknown local wind acceleration, whereas a_{MAX} represents its maximum intensity.

The problem is therefore formulated to find the minimum of J with constraints expressed by Eq. (20) as follows

$$J_a(\boldsymbol{w}_e, \boldsymbol{w}_e) = J + \frac{1}{2}\int_0^T \boldsymbol{\lambda}^T(\boldsymbol{w}_e - \boldsymbol{a})\,\mathrm{d}t$$

$$\equiv \frac{1}{2}\int_0^T L(\boldsymbol{w}_e, \boldsymbol{w}_e)\,\mathrm{d}t = \min \tag{21}$$

with

$$L(\boldsymbol{w}_e, \boldsymbol{w}_e) = [\boldsymbol{z}(t) - \boldsymbol{y}_e]^T \boldsymbol{R}^{-1}[\boldsymbol{z}(t) - \boldsymbol{y}_e] + \boldsymbol{\lambda}^T(\boldsymbol{w}_e - \boldsymbol{a}) \tag{22}$$

where L is a function of both $\boldsymbol{w}_e$ and $\boldsymbol{w}_e$, whereas $\boldsymbol{\lambda}$ is the Lagrange multipliers vector. The solution that minimizes J is obtained applying the variational calculus to Eq. (21), that is,

$$\frac{\mathrm{d}}{\mathrm{d}t}\left(\frac{\partial L}{\partial \boldsymbol{w}_e}\right) - \frac{\partial L}{\partial \boldsymbol{w}_e} = 0, \qquad \boldsymbol{\lambda}^T\boldsymbol{a} = \max, \qquad \sqrt{\boldsymbol{a}^T\boldsymbol{a}} \leq a_{\mathrm{MAX}} \tag{23}$$

Introducing Eq. (22) into Eq. (23), one obtains the following system:

$$\boldsymbol{\lambda} = \boldsymbol{R}^{-1}\frac{\partial \boldsymbol{g}_{\mathrm{NN}}}{\partial \boldsymbol{w}_e} \tag{24}$$

$$\boldsymbol{\lambda}^T\boldsymbol{a} = \max, \qquad \sqrt{\boldsymbol{a}^T\boldsymbol{a}} \leq a_{\mathrm{MAX}} \tag{25}$$

where Eq. (24) gives the time history of $\boldsymbol{\lambda}$, and the algebraic set of Eq. (25) gives the value of $\boldsymbol{a}$. Then Eqs. (24) and (25) can be rewritten as

$$\boldsymbol{\lambda} = \boldsymbol{R}^{-1}\frac{\partial \boldsymbol{g}_{\mathrm{NN}}}{\partial \boldsymbol{w}_e} \tag{26}$$

$$\boldsymbol{w}_e = a_{\mathrm{MAX}}\frac{\boldsymbol{\lambda}}{|\boldsymbol{\lambda}|} \tag{27}$$

Equation (27) states that $\boldsymbol{w}_e$ describes in the space (a_{Wx}, a_{Wy}, a_{Wz}) the points of a sphere having radius a_{MAX} and center in the origin $(0, 0, 0)$. Because of the presence of a discontinuity of the term $\boldsymbol{\lambda}/|\boldsymbol{\lambda}|$ in the origin, Eq. (27) does not admit solutions representing steady winds. To obtain steady solutions, in Eq. (27), a_{MAX} is replaced by the term $a_{\mathrm{MAX}}\tanh(|\boldsymbol{\lambda}|)$, which is a function that vanishes at $|\boldsymbol{\lambda}| = 0$ and is equal to a_{MAX} when $|\boldsymbol{\lambda}| \to \infty$:

$$\boldsymbol{\lambda} = \boldsymbol{R}^{-1}\frac{\partial \boldsymbol{g}_{\mathrm{NN}}}{\partial \boldsymbol{w}_e}, \qquad \boldsymbol{w}_e = a_{\mathrm{MAX}}\tanh(|\boldsymbol{\lambda}|)\frac{\boldsymbol{\lambda}}{|\boldsymbol{\lambda}|} \tag{28}$$

allowing steady solutions for $|\boldsymbol{\lambda}| \to 0$.

As a conclusion, the problem has been reduced to a set of ordinary differential equations, the solutions of which give the time histories of $\boldsymbol{w}_e$ and $\boldsymbol{\lambda}$. In particular, $\boldsymbol{w}_e$ and $\boldsymbol{\lambda}$ are calculated integrating Eqs. (28), and, therefore, they depend upon the initial condition $\boldsymbol{w}_e(t = 0)$, $\boldsymbol{\lambda}(t = 0)$. In all of the calculations, it is $\boldsymbol{w}_e(t = 0) = 0$, $\boldsymbol{\lambda}(t = 0) = 0$.

Also, a_{MAX} has the purpose to limit fast time variations of the estimated gust speed, and an adequate value of it prevents undesirable reproductions of noises and turbulent velocity fluctuations.

Filtering Approach for Wind-Velocity Estimation

To validate the proposed method, the results calculated by the VT approach will be compared with those of a classical technique based on filtering approach, which is described in the present section.

The scheme of filtering approach[6,7] is shown in Fig. 3, where the wind estimation is carried out by modeling the three wind-velocity components as state parameters that satisfy the following equation:

$$\boldsymbol{w} = 0 \tag{29}$$

By defining the augmented state vector $\boldsymbol{x}_a^T = (\boldsymbol{x}^T, \boldsymbol{w}^T)$, the equations of the augmented system read as follows[6,7,13]:

$$\boldsymbol{x}_a = \begin{bmatrix} \boldsymbol{f}(\boldsymbol{x}, \boldsymbol{u}, \boldsymbol{w}, \boldsymbol{\eta}) \\ 0 \end{bmatrix}, \qquad \boldsymbol{y} = \boldsymbol{h}(\boldsymbol{x}, \boldsymbol{u}), \qquad \boldsymbol{z} = \boldsymbol{y} + \boldsymbol{\xi} \tag{30}$$

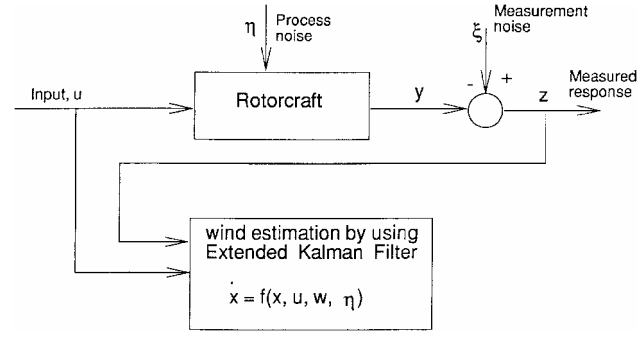

Fig. 3 Scheme of the filtering approach (KF).

The wind estimation is carried out applying the extended steady-state Kalman filter to Eq. (30). To calculate the Kalman filter, the linearized version of Eq. (30) is considered:

$$\boldsymbol{x}_a = \boldsymbol{A}\boldsymbol{x} + \boldsymbol{B}\boldsymbol{u} + \boldsymbol{H}\boldsymbol{w} + \boldsymbol{F}\boldsymbol{\eta} + \boldsymbol{b}_x$$

$$\boldsymbol{y} = \boldsymbol{C}\boldsymbol{x} + \boldsymbol{D}\boldsymbol{u} + \boldsymbol{b}_y, \qquad \boldsymbol{z} = \boldsymbol{y} + \boldsymbol{\xi} \tag{31}$$

where $\boldsymbol{b}_x$ and $\boldsymbol{b}_y$ are bias terms that take into account nonzero initial conditions and possible systematic errors.

The procedure calculates the steady-state Kalman matrix gain as[6,7]

$$\boldsymbol{K} = \boldsymbol{P}\boldsymbol{C}\boldsymbol{R}^{-1} \tag{32}$$

where $\boldsymbol{P}$ satisfies the well-known algebraic Riccati equation

$$\boldsymbol{A}\boldsymbol{P} + \boldsymbol{P}\boldsymbol{A}^T - \boldsymbol{P}\boldsymbol{C}^T\boldsymbol{R}^{-1}\boldsymbol{C}\boldsymbol{P} + \boldsymbol{F}\boldsymbol{V}\boldsymbol{F}^T = 0 \tag{33}$$

Hence, the augmented estimated state is calculated by solving the differential system

$$\boldsymbol{x}_{\text{ae}} = \begin{bmatrix} \boldsymbol{f}(\boldsymbol{x}_e, \boldsymbol{u}, \boldsymbol{w}_e, 0) \\ 0 \end{bmatrix} + \boldsymbol{K}(\boldsymbol{y} - \boldsymbol{h}) \tag{34}$$

Next, the Kalman matrix gain is splitted in the two submatrices $\boldsymbol{K}_x$ and $\boldsymbol{K}_w$ such that $\boldsymbol{K} = (\boldsymbol{K}_x \boldsymbol{K}_w)^T$, so as to separate the wind-velocity equations from the other ones:

$$\boldsymbol{x}_e = \boldsymbol{f}(\boldsymbol{x}_e, \boldsymbol{u}, \boldsymbol{w}_e, 0) + \boldsymbol{K}_x(\boldsymbol{y} - \boldsymbol{h}), \qquad \boldsymbol{w}_e = \boldsymbol{K}_w(\boldsymbol{y} - \boldsymbol{h}) \tag{35}$$

Finally, the time history of $\boldsymbol{x}_e$ and $\boldsymbol{w}_e$ are obtained by integrating Eqs. (35), which that therefore need initial conditions on both $\boldsymbol{x}_e$ and $\boldsymbol{w}_e$.

As for the implementation of this procedure, a few remarks follows. The Runge–Kutta fourth-order method with adaptive time step is used to integrate Eqs. (35). Because the extended Kalman filter method is applied to a nonlinear system, it is necessary to calculate both state and control matrices several times during the simulations. The method checks all of the state variables, and, when the maximum of their relative variations exceeds 0.05 of the reference value, it updates the matrices $\boldsymbol{A}$, $\boldsymbol{B}$, $\boldsymbol{H}$, $\boldsymbol{F}$, and $\boldsymbol{K}$. Greater allowed variation of the state variables does not always permit the convergence of the procedure. The matrices that appear in Eqs. (31) are calculated using centered finite differences, Eq. (33) is solved by a subroutine based on the Newton–Raphson algorithm, and, in all of the simulations, the initial condition of Eqs. (35) is assumed to be $\boldsymbol{x}_e(t = 0) = \boldsymbol{x}(t = 0)$ and $\boldsymbol{w}_e(t = 0) = 0$.

Results and Discussion

The effectiveness of the proposed method is evaluated by carrying out simulations wherein the motion of the rotorcraft in the presence of wind is considered. The results so obtained are compared with the corresponding calculations realized applying the extended Kalman filter method.

In all of the simulations run by using VT, the components in body axes of the acceleration are measurable, whereas all of the state variables are supposed to be observable from the simulations. So that in Eqs. (10) and (12), it is $\boldsymbol{g} = (a_x, a_y, a_z)$. As a consequence, in Eq. (18), $\boldsymbol{R}$ is a 3×3 diagonal matrix, the elements of which represent the standard deviations of the acceleration measurement errors. In all of the simulations, the elements of $\boldsymbol{R}$ are given by realistic values based on sensor characteristics, and it results $R_{11} = R_{22} = R_{33} = 0.05\ \text{ms}^{-2}$.

The value for a_{MAX} is to be selected so as to keep an accurate estimation of the mean wind velocity and an adequate filtering on the turbulent fluctuations. In this respect $a_{\text{MAX}} = 1\ \text{ms}^{-2}$ appears to satisfy both the requirements because, according to simulations, it provides an acceptable filtering effect together with a good evolution of the mean velocity variations. Higher values of a_{MAX} cause undesirable reproductions of turbulent fluctuations, whereas lower values can result in excessively slow estimation of the mean wind velocity.

In Eqs. (31) and (32) $\boldsymbol{C}$ is a 12×12 identity matrix, and $\boldsymbol{R}$ is assumed to be a 12×12 diagonal matrix whose elements are given by realistic values based on the sensors characteristics. They are $R_{11} = R_{22} = R_{33} = 0.1\ \text{ms}^{-1}$, $R_{44} = R_{55} = R_{66} = 0.02$ rad, $R_{77} = R_{88} = R_{99} = 0.03\ \text{rad s}^{-1}$, $R_{10\,10} = R_{11\,11} = 5$ m, and $R_{12\,12} = 50$ m. The subscript number indicates the corresponding state variable, and, also in this case, all of the elements are chosen considering the measurement error.

In all of the simulations, it is assumed that the noise $\boldsymbol{\eta}$ is caused by the atmospheric turbulence.

To compare the two algorithms, five cases will be considered where the initial condition for the simulation is a level flight with a speed equal to $30\ \text{ms}^{-1}$ at an altitude of 100 m.

The first case, addressed in Fig. 4, considers a simulation lasting 20 s where the rotorcraft, after 5-s, encounters an ascending

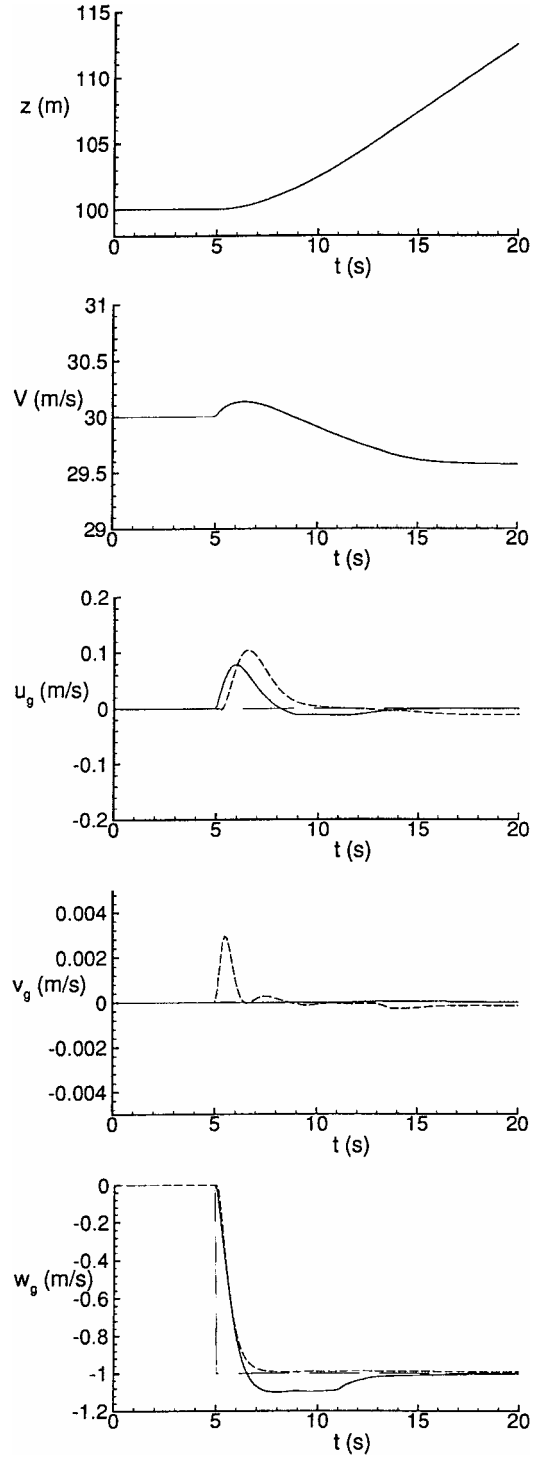

Fig. 4 Case 1: wind-velocity time histories for a vertical gust; $w_g = -1\ \text{ms}^{-1}$.

gust having velocity equal to 1 ms^{-1}. The two algorithms achieve the same asymptotical values of wind velocities, but, whereas KF method (dashed line) generates a time history in which w_g monotonically approaches the limit of -1 ms^{-1}, the VT time history (continuous line) presents an overshoot with respect to the real wind velocity (dotted line). The choice of a_{MAX} for VT and $\boldsymbol{R}$ for KF leads to time histories that, after 5 s, present very similar slopes of w_g. The maximum errors on the component u_g result in 0.09 ms^{-1} and 0.11 ms^{-1} for the VT and KF respectively, whereas the errors of v_g are always less than 0.005 ms^{-1} for both the algorithms. Although both rotorcraft motion and gust velocity distribution are two dimensional, the KF method yields values of v_g slightly different from zero. This is because the wind estimation is realized by means of the Kalman filter applied to a complete set of the equations of motion, which, in general, do not guarantee the calculation of the exact value of the wind velocity.

In the second simulation the vehicle flies into a vertical turbulent gust described by the Dryden model. The turbulence scale is assumed to be equal to 100 m, whereas $\langle u_g \rangle = \langle v_g \rangle = 0$, $\langle w_g \rangle = 1$ ms^{-1} and $\sigma_x = \sigma_y = 0$, $\sigma_z = 0{\cdot}2$ ms^{-1}. The elements of $\boldsymbol{V}$ are $V_{11} = \sigma_x^2$, $V_{22} = \sigma_y^2$, $V_{33} = \sigma_z^2$, and $V_{ij} = 0$, $i \neq j$, whereas the turbulence scale is assumed on the basis of the data reported in Ref. 10. Figure 5 illustrates the time histories of various quantities such as altitude, vehicle speed, and wind-velocity components, whereas Table 2 reports estimated average velocities and standard deviations of the velocities. It appears from Table 2 that the estimate errors of w_g are about 4.5 and 3% for VT and KF, respectively. Also in this two-dimensional case, values of v_g slightly different from zero are computed from the KF procedure.

The third case concerns a more complex situation, where the vehicle flies into an atmospheric region with a uniform mean velocity distribution and an appreciable turbulent level, which is, also in this case, described by means of the Dryden model, with $\sigma_x = \sigma_y = \sigma_z = 0{\cdot}2$ ms^{-1}, $\langle u_g \rangle = \langle v_g \rangle = 1$ ms^{-1}, $\langle w_g \rangle = -1$ ms^{-1}, and a turbulence scale of 100 m. Hence $\boldsymbol{V}$ is expressed by $V_{11} = \sigma_x^2$, $V_{22} = \sigma_y^2$, $V_{33} = \sigma_z^2$, and $V_{ij} = 0$, $i \neq j$. Figure 6 shows the wind-velocity components vs time, whereas Table 3 gives the average velocities and the standard deviations obtained with the two procedures. The maximum difference between true and estimated velocities are less than 4 and 6% for the VT and KF methods, respectively.

The fourth case, shown in Fig. 7, regards a simulation lasting 50 s where the wind velocities are variable. Wind components in a three-dimensional gust are expressed as follows:

$$u_g = 2\sin^2(2\pi t/T_m), \qquad v_g = 0{\cdot}5,\ t > 0$$
$$w_g = -\sin(2\pi t/T_m) \tag{36}$$

where $T_m = 50$ s is equal to the entire simulation period. The analysis of the time histories shows that KF and VT adequately reproduce the three wind-velocity components, and their errors are always less than 6 and 5%, respectively.

Table 2 Case 2: Mean values and standard deviations of wind velocities

Parameter	Nominal	VT	KF
$\langle u \rangle$	0.00	$-1.43E-3$	$8.4E-3$
$\langle v \rangle$	0.00	$1.6E-5$	$1.4E-4$
$\langle w \rangle$	-1.00	-0.9706	-0.9552
σ_x	0.00	0.0151	0.0342
σ_y	0.00	$4.66E-5$	$2.1E-3$
σ_z	0.20	0.169	0.151

Table 3 Case 3: Mean values and standard deviations of wind velocities

Parameter	Nominal	VT	KF
$\langle u \rangle$	1.00	1.027	0.9980
$\langle v \rangle$	1.00	0.977	0.9583
$\langle w \rangle$	-1.00	-0.967	-0.9437
σ_x	0.20	0.176	0.178
σ_y	0.20	0.186	0.140
σ_z	0.20	0.150	0.153

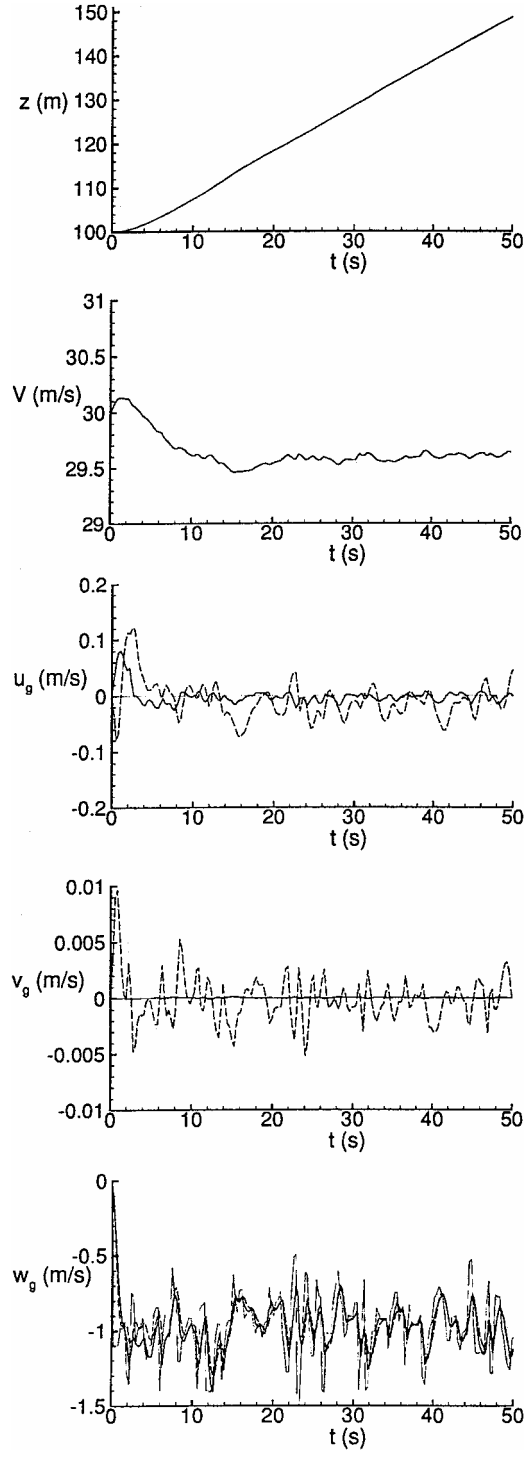

Fig. 5 Case 2: wind-velocity time histories for a vertical gust in the presence of turbulence; $\langle u_g \rangle = \langle v_g \rangle = 0$, $\langle w_g \rangle = -1$ ms^{-1}, $\sigma_x = \sigma_y = 0$, and $\sigma_z = 0.2$ ms^{-1}.

Figure 8 illustrates the fifth case that corresponds to a flight into a turbulent gust having the aforementioned mean velocity distributions but in the presence of a significant turbulent level given by the following standard deviations $\sigma_x = 0{\cdot}2$ ms^{-1}, $\sigma_y = 0{\cdot}05$ ms^{-1}, $\sigma_z = 0{\cdot}1$ ms^{-1}, so that $V_{11} = \sigma_x^2$, $V_{22} = \sigma_y^2$, $V_{33} = \sigma_z^2$, and $V_{ij} = 0$, $i \neq j$, with a turbulence scale equal to 100 m. In spite of the simultaneous presence of turbulence effects and time variations of mean velocity, it is possible to distinguish the mean velocity from the turbulent fluctuations in the time histories obtained by the two algorithms.

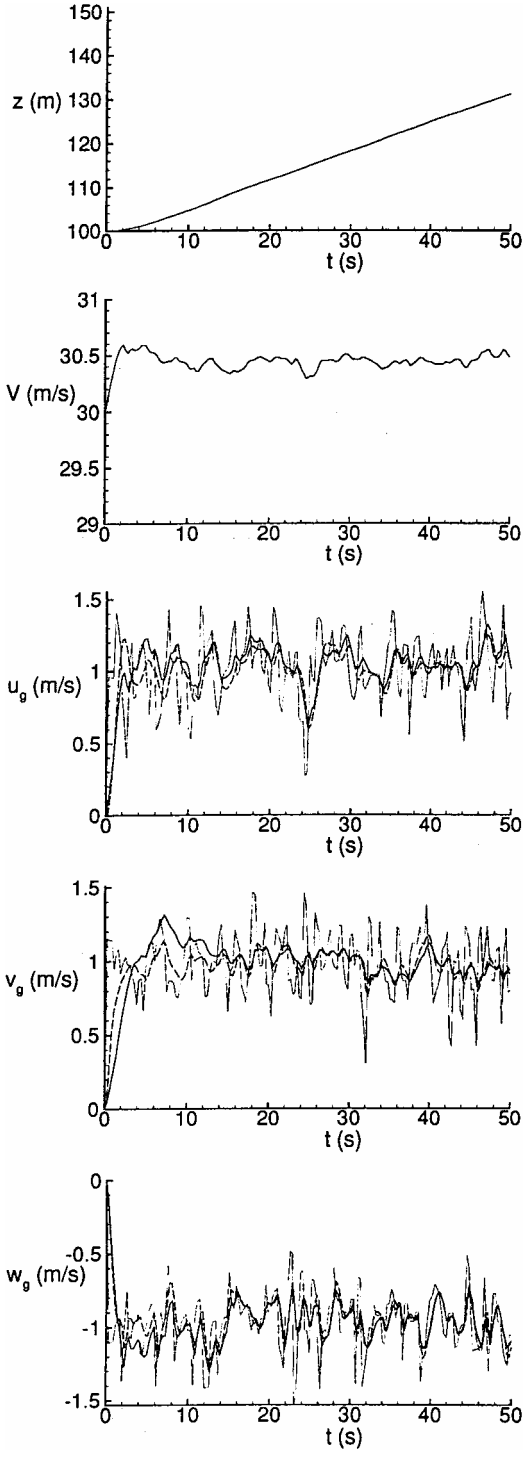

Fig. 6 Case 3: wind-velocity time histories for a steady gust in the presence of turbulence; $\langle u_g \rangle = \langle v_g \rangle = 1$ ms^{-1}, $\langle w_g \rangle = -1$ ms^{-1}, and $\sigma_x = \sigma_y = \sigma_z = 0.2$ ms^{-1}.

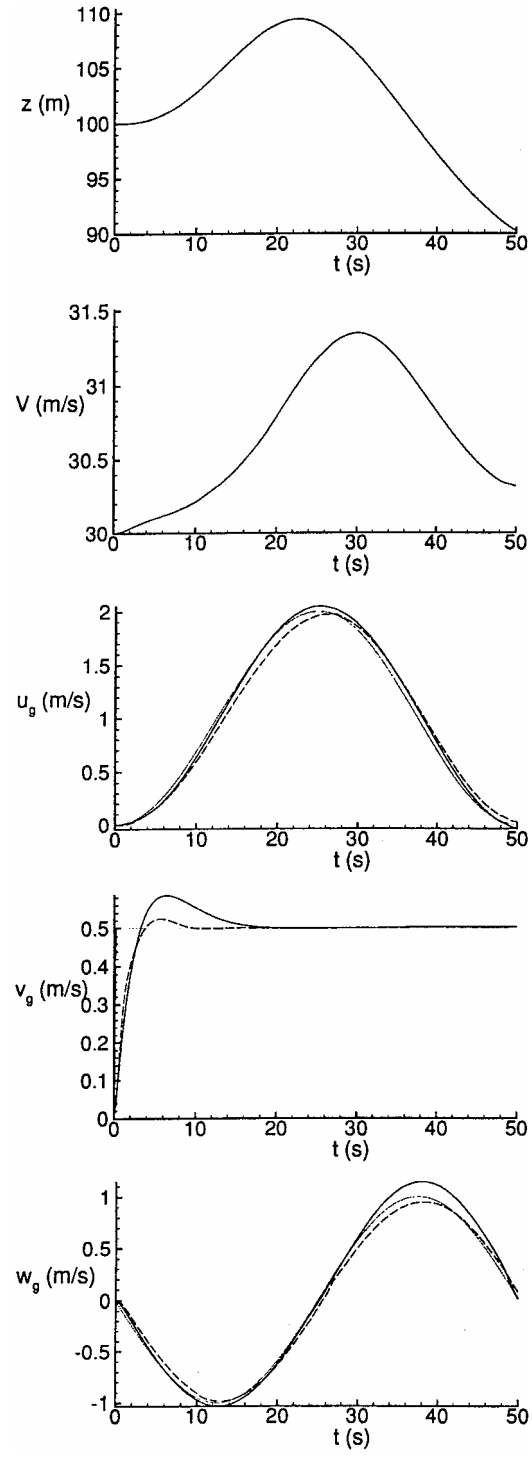

Fig. 7 Case 4: wind-velocity time histories for a three-dimensional variable gust.

Although it is apparent that the two methods produce very similar results, a sizeable difference can be observed from the computational point of view. In all of the simulations, VT is resulted about two to three times faster than KF, and this is related to the different computational tasks that occur in the two procedures.

In fact, the VT method requires the calculation of $\boldsymbol{g}_{\mathrm{NN}}$ and its derivatives with respect to $\boldsymbol{w}_e$, the determination of Lagrange multipliers, and estimated wind velocities. While in the KF technique, it is necessary to evaluate many times during the simulation $\boldsymbol{A}$, $\boldsymbol{B}$, $\boldsymbol{H}$, $\boldsymbol{F}$ and $\boldsymbol{K}$ because of the nonlinearities in the vehicle model.

Because of the use of artificial neural networks together with the assumption of constant rotary and control derivatives, the computed wind velocities can slightly differ with respect to the exact values. Of course, these differences are more limited if all of the neural networks are properly trained.

The advantage of VT with respect to KF is that the method does not require the linearization of the equations of motion, whereas the KF technique requires the calculation of state and control matrices and Kalman matrix gain. Furthermore, the VT method only calculates the time variations of the Lagrange multipliers associated to the wind-velocity components, whereas the KF approach requires the calculation of the estimated state $\boldsymbol{x}_e$.

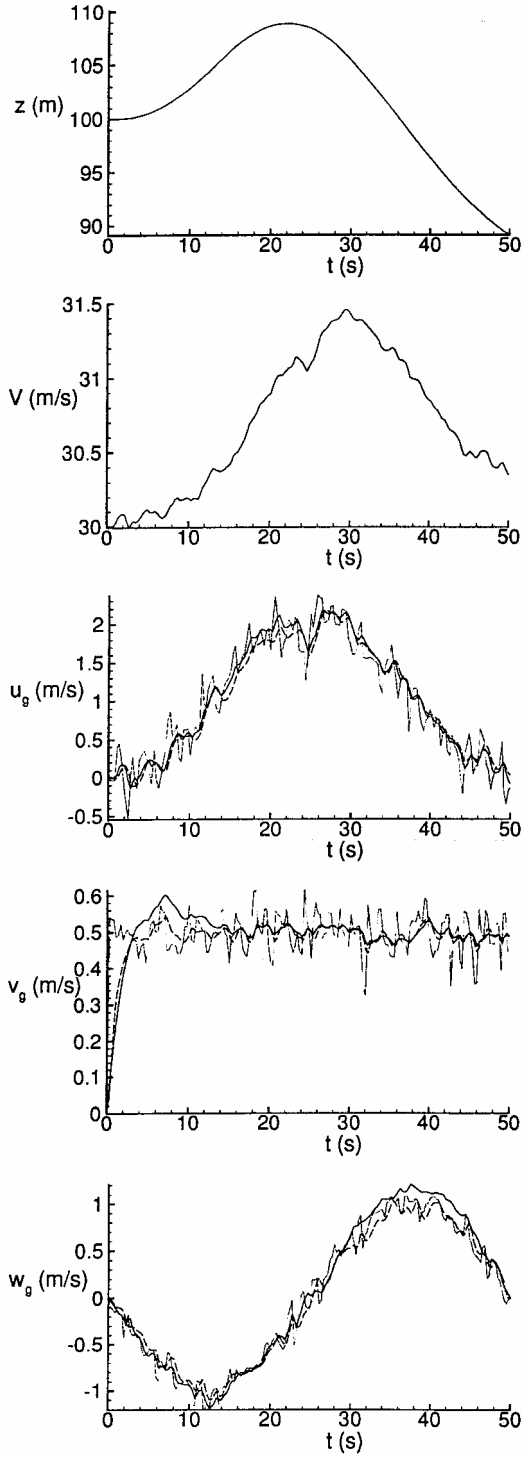

Fig. 8 Case 5: wind-velocity time histories for a three-dimensional variable gust in the presence of turbulence.

If, in the KF method, $\boldsymbol{H}$, $\boldsymbol{F}$, and $\boldsymbol{K}$ were a priori scheduled with the slow state variables (airspeed and altitude), the procedure would be more efficient. Nevertheless, several tests have shown that, because of the strong nonlinearities of the model, the scheduled Kalman filter calculates velocities that do not always tend to the real value of the wind velocity.

For VT, $\boldsymbol{g}_{NN}$ must be necessarily a nontrivial function of the wind velocities in such a way that its derivatives with respect to wind velocity are not zero. For this reason $\boldsymbol{g}$ has been assumed to be equal to the vehicle acceleration.

On the other hand, in the KF method the observability function depends on the state and control variables only. This, in general, makes the VT approach less adaptable than the filtering approach method.

The main limitation of the VT is that all of the state variables have to be measurable, a situation that is very difficult to realize in practical applications. To avoid this restriction, the filtering approach could be used to estimate efficiently the vehicle state, whereas the wind estimation can be interfaced with the state estimation filter.

Conclusions

This work concerns the problem of wind estimation through the measurements of the state variables of a shrouded-fan unmanned-aerial-vehicle rotorcraft. The motivation of the study is related to the difficulties of the wind measurements aboard on a rotary-wing vehicle as a result of the influence of the rotor flow on the aerodynamic field about the vehicle.

A variational technique is proposed for the estimation of the wind velocity components. The approach is based on adjoint differential equations that reasonably describe the wind-velocity evolution.

Comparison with a Kalman filter technique has shown that the proposed algorithm provides good results together with a considerable saving of computational time. A final conclusion regards the main limitation of the proposed method that consists in the fact that the measurability of the full state is required.

Acknowledgment

This work was partially supported by Italian Ministry of University.

References

[1]Walsh, D., and Cycon, J. P., "The Sikorsky Cypher UAV: A Multi-Purpose Platform with Demonstrated Mission Flexibility," *Proceedings of the Annual Helicopter Society 54th Annual Forum*, Washington, DC, May 1998, pp. 1410–1418.

[2]de Divitiis, N., "Aerodynamic Modeling and Performance Analysis of a Shrouded Fan Unmanned Aerial Vehicle," International Council of the Aeronautical Sciences, Paper 256, Sept. 2002.

[3]Avanzini, G., D'Angelo, S., and de Matteis, G., "Performance and Stability of a Ducted-Fan Uninhabited Aerial Vehicle Model," *Journal of Aircraft*, Vol. 40, No. 1, 2003, pp. 86–93.

[4]Lamb, H., "On the Motion of Solids Through a Liquid," *Hydrodynamics*, 6th ed., edited by Dover, New York, 1945, pp. 160–201.

[5]Katz, A., and Sharma, M., "Estimation of Wind from Airplane State in Coordinated Flight," *Journal of Aircraft*, Vol. 35, No. 2, 1998, pp. 191–196.

[6]Hamel, P. G., and Jategaonkar, R. V., "Evolution of Flight Vehicle System Identification," *Journal of Aircraft*, Vol. 33, No. 1, 1996, pp. 9–28.

[7]Jategaonkar, R. V., and Plaetschke, E., "Algorithms for Aircraft Parameter Estimation Accounting for Process and Measurement Noise," *Journal of Aircraft*, Vol. 26, No. 4, 1988, pp. 360–372.

[8]McCool, K. M., Haas, D. J., and Schaefer, C. G., "A Neural Network Based Approach to Helicopter Low Airspeed and Sideslip Angle Estimation," AIAA Paper 96-3481-CP, July 1996.

[9]McMillen, R. L., Steck, J. E., and Rokhsaz, K., "Application of an Artificial Neural Network as a Flight Test Data Estimator," *Journal of Aircraft*, Vol. 32, No. 5, 1995, pp. 1088–1094.

[10]Etkin, B., *Dynamics of Atmospheric Flight*, Wiley, New York, 1972, pp. 104, 152.

[11]"VSAERO User's Manual," Analytical Methods Inc. Rev. E5, Seattle, April 1994, pp. 1–52.

[12]Padfield, G., *Helicopter Flight Dynamics: The Theory and Application of Flying Qualities and Simulation Modeling*, AIAA, Reston, VA, 1996, pp. 9–85.

[13]Friedland, B., *Control System Design*, McGraw–Hill, New York, 1986, pp. 337, 347.